

1 E06-014

A Precision Measurement of d_2^n : Probing the Lorentz Color Force

S. Choi, X. Jiang, Z.-E. Meziani, B. Sawatzky, spokespersons, and
the d_2^n and Hall A Collaborations.
Contributed by D. Flay.

1.1 Overview

1.1.1 Physics Motivation

To date, extensive work has been done investigating the spin structure function g_1 within the context of the Feynman Parton Model and pQCD. However, far less is known about the g_2 structure function. It is known to contain quark-gluon correlations, and its study could possibly yield a better understanding of the nature of confinement. It represents a spin-flip Compton amplitude, and may be written as:

$$g_2(x, Q^2) = g_2^{WW}(x, Q^2) + \bar{g}_2(x, Q^2), \quad (1)$$

where g_2^{WW} is the Wandzura-Wilczek term, which may be expressed entirely in terms of g_1 [1]:

$$g_2^{WW}(x, Q^2) = -g_1(x, Q^2) + \int_x^1 \frac{g_1(y, Q^2)}{y} dy. \quad (2)$$

The second term is given as:

$$\bar{g}_2(x, Q^2) = - \int_x^1 \frac{1}{y} \frac{\partial}{\partial y} \left[\frac{m_q}{M} h_T(y, Q^2) + \xi(y, Q^2) \right] dy, \quad (3)$$

where h_T is the transverse polarization density, and ξ is a twist-3 dominated term arising from quark-gluon correlations. Here, h_T is suppressed by the ratio of the quark mass m_q to that of the target mass M . Therefore, a measurement of \bar{g}_2 provides access to twist-3 effects inside the nucleon [2].

Subsequently, a measurement of both g_1 and g_2 allows for the determination of the quantity d_2^n , which is formed as the second moment of a linear combination of g_1 and g_2 :

$$d_2^n(Q^2) = \int_0^1 x^2 [2g_1(x, Q^2) + 3g_2(x, Q^2)] dx = 3 \int_0^1 x^2 \bar{g}_2(x, Q^2) dx. \quad (4)$$

d_2^n also appears as a matrix element in the operator product expansion [3]:

$$g \langle P, S | \bar{\psi}_q(0) G^{+y}(0) \gamma^+ \psi_q(0) | P, S \rangle = 2MP^+ P^+ S^x d_2^n, \quad (5)$$

where $G^{+y} = \frac{1}{\sqrt{2}}(B^x - E^y)$. We see from Eq. 4 that d_2^n is a direct measure of quark-gluon interactions. Eq. 5 may be written in component form,

$$\langle P, S | \psi_q^\dagger \vec{\alpha} \times g \vec{E} \psi_q | P, S \rangle = 2M^2 \chi_E \vec{S} \quad \text{and} \quad \langle P, S | \psi_q^\dagger g \vec{B} \psi_q | P, S \rangle = 2M^2 \chi_B \vec{S}, \quad (6)$$

from which d_2^n may be written as $d_2^n = \frac{1}{8}(\chi_E + 2\chi_M)$.

In the limit of low Q^2 where the virtual photon wavelength is larger than the nucleon size, the electromagnetic field of the virtual photons associated with g_2 in the interaction will appear as uniform over the nucleon volume. Consequently, d_2^n is seen to be connected with spin polarizabilities [4].

Recent work has shown [4, 5] that at high Q^2 , d_2^n is more appropriately seen as a color Lorentz force averaged over the volume of the nucleon. This is given by the expression of the transverse (color) force on the active quark immediately following its interaction with a virtual photon:

$$F^y(0) \equiv -\frac{\sqrt{2}}{2P^+} \langle P, S | \bar{\psi}_q(0) G^{+y}(0) \gamma^+ \psi_q(0) | P, S \rangle = -\frac{1}{2} M^2 d_2^n. \quad (7)$$

This theoretical interpretation reveals how g_2 and subsequently d_2^n will allow us to examine some of the properties of confinement with great precision.

1.1.2 Current Status and Goals

While bag and soliton model calculations of d_2 for the neutron yield numerical values consistent with those of Lattice QCD, current experimental data differs by roughly two standard deviations. One of the intentions of our experiment is to improve the experimental error on the value of d_2^n by a factor of four. It subsequently provides a benchmark test on Lattice QCD calculations.

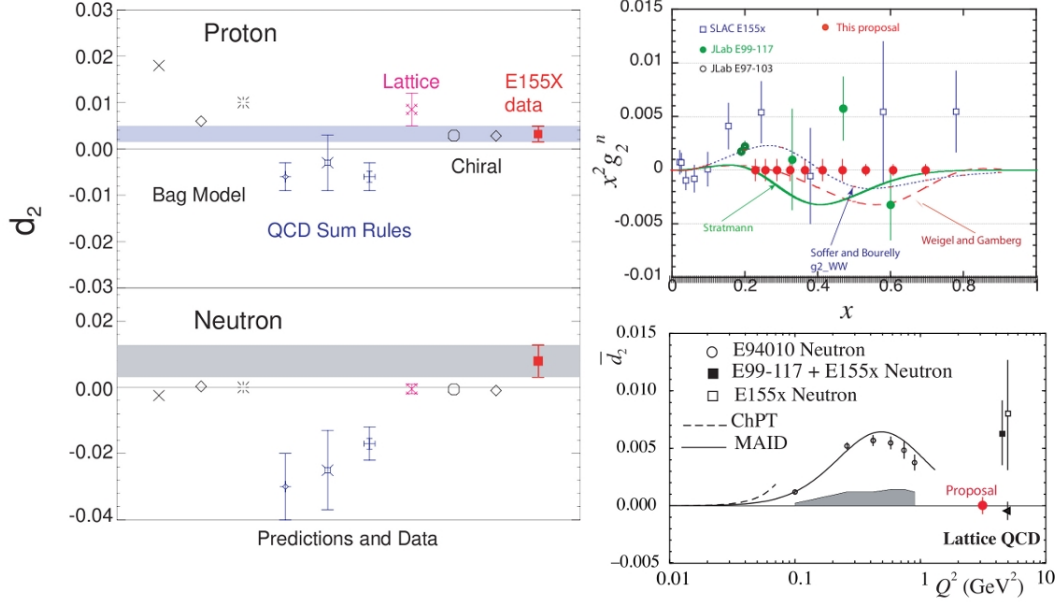


Figure 1: On the left is the current world data on d_2 [6]. There is a need for more precise neutron data, which E06-014 addresses. On the right is the projected error on both $g_2(x)$ (top) and $d_2^n (\approx 3\text{GeV}^2)$ (bottom).

1.2 The Experiment

The experiment ran in Hall A of Jefferson Lab from February to March of 2009, with two beam energies of $E = 4.73$ and 5.89 GeV, covering the resonance and deep inelastic valence quark regions, characterized by $0.2 \leq x \leq 0.7$ and $2 \leq Q^2 \leq 6$ GeV².

In order to calculate d_2^n , we scattered a longitudinally polarized electron off of a ^3He target, in two polarization configurations – longitudinal and transverse. ^3He serves as an effective neutron target since roughly 86% of the polarization is carried by the neutron. This is due to the two protons in the nucleus being primarily bound in a spin singlet state [7, 8].

We measured the unpolarized total cross section σ_0 and the asymmetries A_{\parallel} and A_{\perp} . The cross section was measured by the Left High-Resolution Spectrometer (LHRS), while the asymmetries were measured by the BigBite Spectrometer. Both the LHRS and BigBite were oriented at scattering angles of $\theta = 45^\circ$ to the left and right of the beamline, respectively.

Expressing the structure functions entirely in terms of these experimental quantities, we have the expression for d_2^n :

$$d_2^n = \int_0^1 \frac{MQ^2}{4\alpha^2} \frac{x^2 y^2}{(1-y)(2-y)} \sigma_0 \left[\left(3 \frac{1+(1-y)\cos\theta}{(1-y)\sin\theta} + \frac{4}{y} \tan(\theta/2) \right) A_{\perp} + \left(\frac{4}{y} - 3 \right) A_{\parallel} \right] dx, \quad (8)$$

where $x = Q^2/2M\nu$, $\nu = E - E'$ is the energy transfer to the target, E' is the scattered electron energy, and $y = \nu/E$ is the fractional energy transfer to the target. The asymmetries are given by:

$$A_{\parallel} = \frac{\sigma^{\downarrow\uparrow} - \sigma^{\uparrow\uparrow}}{2\sigma_0} \quad \text{and} \quad A_{\perp} = \frac{\sigma^{\downarrow\Rightarrow} - \sigma^{\uparrow\Rightarrow}}{2\sigma_0}.$$

1.3 Analysis Progress

1.3.1 The Left High-Resolution Spectrometer

Before we can begin to identify particles in the LHRS, we need to calibrate our detectors. Both the gas Čerenkov and the pion rejector have been calibrated so that we may be able to discern electrons from pions.

First, each of the ten photomultiplier tubes (PMTs) in the gas Čerenkov were gain-matched by use of our Hall A Analyzer database, so that each of their one photoelectron peaks aligns to a specified value in their corresponding ADC spectrum. This allows us to determine the average photoelectron yield of each PMT. In the pion rejector, a similar process was followed for each PMT corresponding to each of the thirty four blocks in each layer of the pion rejector. We used the gas Čerenkov to identify pions in the pion rejector, and gain-matched each block's pion ADC spectrum to an arbitrary specified value. This was carried out for one particular momentum setting in the LHRS [9]. The resulting calibration coefficients were then applied to all other kinematics. The calibration is carried out in this fashion since pions will deposit roughly the same amount of energy in the pion rejector regardless of their momentum.

Currently, work is being done to determine the electron detection, pion rejection, and cut efficiencies for both the gas Čerenkov and the pion rejector. Fig. 2 shows the pion rejection (cut) efficiency of the gas Čerenkov in the LHRS. A pion sample is selected in the pion rejector (N_i) and those events that pass the given cut in the Čerenkov (N_f) have their corresponding Čerenkov spectrum plotted. Then the ratio $r = N_f/N_i$ is calculated. The formula for the efficiency of rejecting pions for the particular cut position in the gas Čerenkov is then written as $\epsilon_{\text{cer}}^{\pi\text{-rej.}} = 1 - r$, as this quantity reflects the percentage of pions removed by a cut in the gas Čerenkov. These quantities will be a contributing factor in the determination of the unpolarized total cross section, σ_0 .

Simulation work concerning the pion rejector is also being carried out to better understand the momentum dependence observed in our E/p distribution as a function of p (Fig. 2).

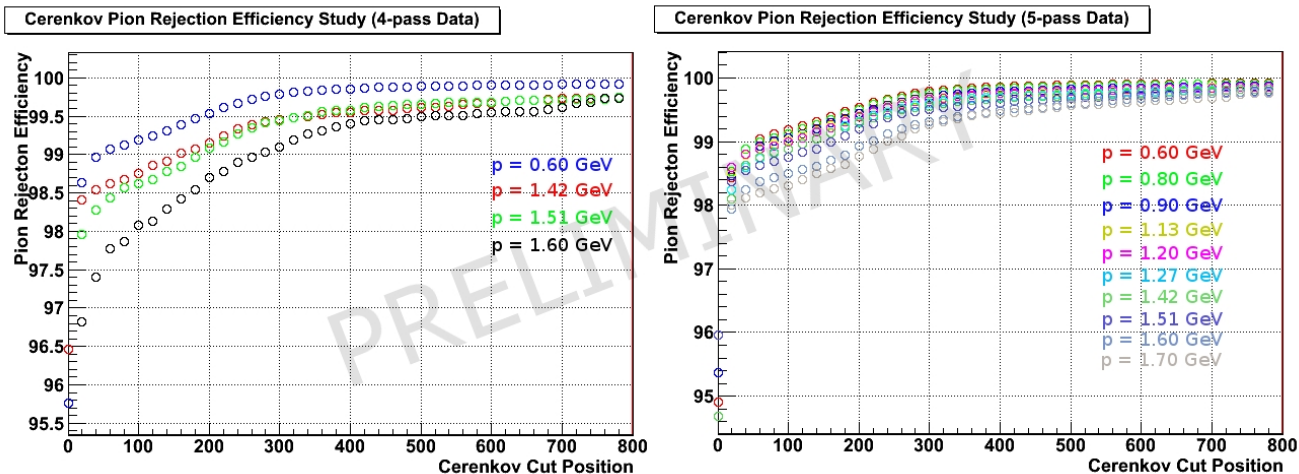


Figure 2: Gas Čerenkov pion rejection efficiency study for 4- and 5-pass data.

1.3.2 The BigBite Spectrometer

In addition to the multiwire drift chambers and the shower calorimeters, this experiment was one of the first to use the gas Čerenkov detector in the BigBite detector package. The Čerenkov detector uses C_4F_{10} as the radiator gas. The Čerenkov radiation is focused from two sets of ten mirrors into twenty PMTs, each of which views one mirror. The Čerenkov detector is needed for electron detection and added pion rejection.

The Čerenkov detector is calibrated by gain-matching the one photoelectron peak for each PMT to a particular ADC channel by adjusting the gain of the PMT during LED runs taken during the running of d_2^n . The photoelectron yield per electron track during the production mode of the experiment is approximately

six. Fig. 3 shows the ADC signal from one of the PMTs. The plot on the left shows an electron signal. The green curve has no TDC cuts, while the blue curve has cuts on the main timing peak of the corresponding TDC spectrum. The red curve has a cut outside the main timing peak in its TDC spectrum. The plot on the right shows the effect of mirror cuts in addition to the aforementioned TDC cuts. The electron signal is shown in green, which requires a reconstructed track to pass through the mirror associated with that particular PMT. The red curve shows background effects, and requires a reconstructed track to *not* pass through the mirror associated with this particular PMT.

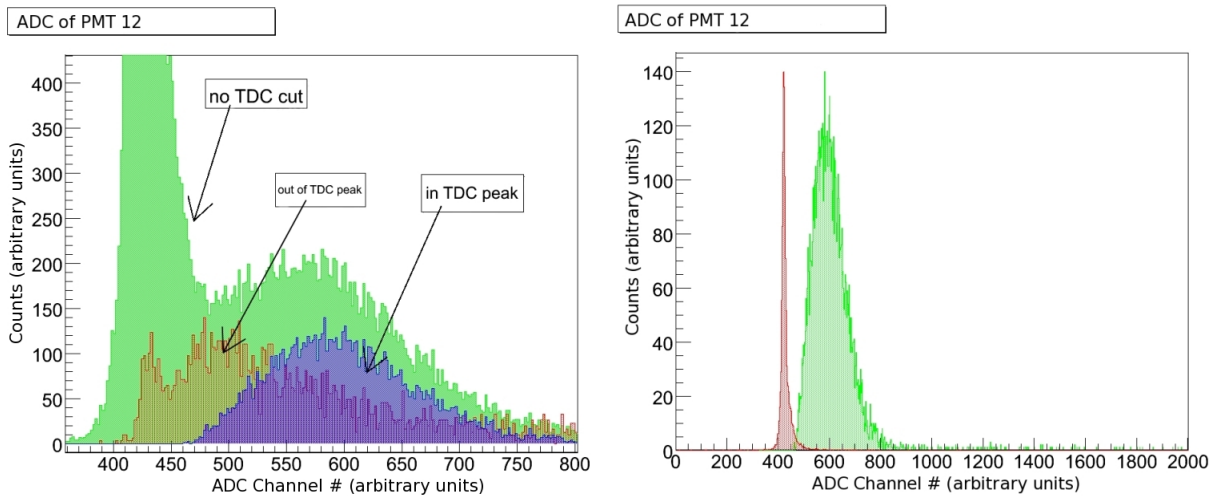


Figure 3: Sample histograms of a calibrated Čerenkov ADC spectrum for one of the mirrors. The plot on the left shows the effect of TDC cuts. The plot on the right shows the effect of TDC and mirror cuts.

Currently, work is being done to calibrate the preshower and shower calorimeters. Once this detector is calibrated, a study of electron detection, pion rejection, and cut efficiencies will be carried out. In addition to identifying electrons for the calculation of the asymmetries A_{\parallel} and A_{\perp} , this study will also determine the magnitude of the pion background which may be removed from the gas Čerenkov and the total shower calorimeter.

1.3.3 The Compton Polarimeter

During the experiment, beam polarization was measured by the Møller polarimeter and by a partially upgraded Compton polarimeter. Although the Compton electron detector was disabled, the photon detector – a single cylinder of GSO crystal – allowed much higher resolution than the lead tungstenate array it replaced, especially at low energies. A comparison between Compton photon data from d_2^B and a Monte Carlo simulation led to the discovery of a misalignment in the Compton photon beamline, which was corrected over the summer.

This experiment also saw the commissioning of a new, integrating data acquisition system for the photon detector signal, as well as a corresponding suite of analysis software. Fig. 4 shows preliminary results from this analysis for a month of d_2^B running. The four accelerator configurations for the experiment – each with a different nominal polarization – can be clearly distinguished. We are refining our Monte Carlo to compute the analyzing power of the Compton polarimeter, which will allow us to translate the raw Compton asymmetries to absolute beam polarizations.

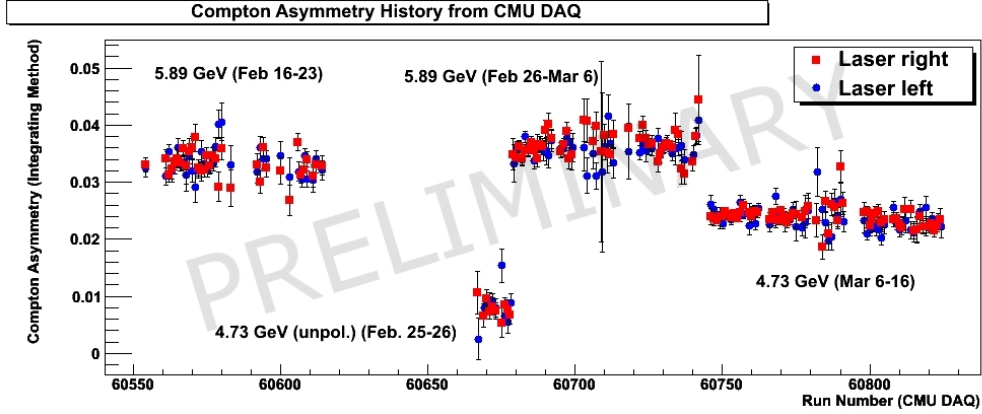


Figure 4: The Compton Asymmetry during the running of d_2^n .

References

- [1] S. Wandzura and F. Wilczek, Phys. Lett. B **72B**, 2 (1977).
- [2] R.L. Jaffe, Comm. Nucl. Part. Phys. **19**, 239 (1990).
- [3] B.W. Filippone and Xiandong Ji, hep-ph/0101224v1.
- [4] M. Burkardt, hep-ph/0905.4079v1.
- [5] M. Burkardt, hep-ph/0902.0163v1.
- [6] S. Choi, Z.-E. Meziani, X Jiang, B. Sawatzky, *et al.*, Jefferson Lab, 2005; PR-06-014.
- [7] J.L. Friar *et al.*, Phys. Rev. C **42**, 6 (1990).
- [8] F. Bissey, A.W. Thomas and I.R. Afnan, Phys. Rev. C **64**, 024004 (2001).
- [9] D. Flay, E06-014 Technical Note, in preparation.